Magnetic anisotropy of bulk GaN:Mn single crystals codoped with Mg acceptors

J. Gosk*
Institute of Experimental Physics, Warsaw University, Hoza 69, 00-681 Warsaw, Poland
and Faculty of Physics, Warsaw University of Technology, Koszykowa 75, 00-662 Warsaw, Poland

M. Zajac, A. Wolos, M. Kaminska, and A. Twardowski
Institute of Experimental Physics, Warsaw University, Hoza 69, 00-681 Warsaw, Poland

I. Grzegory, M. Bockowski, and S. Porowski
High Pressure Research Center, Polish Academy of Sciences, Sokołowska 29/37, 01-142 Warsaw, Poland
(Received 5 July 2004; revised manuscript received 12 November 2004; published 31 March 2005)

Magnetization measurements of the wurtzite highly resistive bulk crystals of GaN:Mn, codoped with Mg, are presented. Strong anisotropy of magnetization at low temperatures (2–10 K) was observed. The data were analyzed assuming Mn ions in d^4 configuration. The crystal field model taking into account cubic field of tetrahedral symmetry, trigonal field along the *c*-axis simulating hexagonal structure, tetragonal static Jahn-Teller distortion, and the spin-orbit interaction provides good description of the experimental magnetization data.

DOI: 10.1103/PhysRevB.71.094432 PACS number(s): 71.55.Eq, 75.30.Gw, 75.50.Pp, 75.10.Dg

I. INTRODUCTION

Recently magnetic semiconductors based on III-V compounds have attracted considerable interest due to potential application of these materials in spintronic devices.[1] Especially attractive is ferromagnetism (FM) observed in InMnAs and GaMnAs,[2,3] as ferromagnetic interaction enhances the effect of external magnetic field. Unfortunately, the observed Curie critical temperatures (T_c) are still far from room temperature, necessary for commercial applications. Some hope was raised by theoretical predictions that T_c can exceed room temperature in *p*-type GaMnN, assuming hole mediated ferromagnetism (Zener model[4]). This suggestion caused GaMnN to become the most intensively studied magnetic III-V material. Ferromagnetism was indeed observed for some GaMnN samples,[5–11] but its origin is still not clear. Some authors relate this FM behavior to GaMnN, while others to FM precipitates in this compound.[9–11] The nature of magnetic interactions in GaMnN, possibly leading to ferromagnetism in this material, is still under discussion. A number of theoretical models for GaMnN were developed.[4,12–17] Important input information for all these models and thus for understanding the magnetic properties of GaMnN is the knowledge about the nature of Mn impurity in GaN.

Manganese impurity in III-V compounds has been studied for a long time. The results of those investigations can be summarized as follows: There are essentially three types of Mn centers in III-V compounds. The first one (we denote it center C1) is formed by substitutional manganese Mn^{3+}, which is in d^4 configuration (the ground state spin $S=2$). This configuration is in fact equivalent to Cr^{2+} in II-VI diluted magnetic semiconductors (DMS), with all the features characteristic for that case, including Jahn-Teller effect (JT) and magnetic anisotropy.[18–20] The second type of Mn center (center C2) constitutes when the center C1 traps an electron and binds it tightly at the *d* shell. Such a center can be regarded as a d^5 configuration, with $S=5/2$. The third type of center results from the fact that the Mn center C2 is negatively charged and can in hand attract and (weakly) bind a hole, forming a (d^5+h) complex (center C3).[21] Due to exchange interaction between the *d* shell ($S=5/2$) and the bound hole ($j=3/2$), the C3 ground state may have a total angular momentum $J=4$ (for ferromagnetic interaction) or $J=1$ (for antiferromagnetic interaction). Centers C1 and C3 can be viewed as neutral acceptor centers A^0 (d^4) and A^0 (d^5+h), respectively, while center C2 as an ionized acceptor A^-.

The nature of the Mn center is crucial for Mn—Mn interaction. C2 centers essentially lead to antiferromagnetic (AFM) superexchange interaction, similarly as for II-Mn-VI compounds. The only hope for ferromagnetism in such a case is high concentration of free carriers (preferably holes), which can induce Zener-type ferromagnetic coupling. On the other hand for C1 centers both AFM and FM exchange channels are possible and the final type of coupling depends on details of energy structure. Moreover coexistence of C1 and C2 centers opens the possibility for a double exchange mechanism, which could yield FM interaction between Mn ions.

The most common configuration of Mn in a III-V compound appears to be C2 center, which was observed for GaMnAs,[22] InMnAs,[23] GaP:Mn,[24] as well as for GaN:Mn.[25] C1 centers were reported for GaP:Mn, for which Mn forms a deep acceptor level.[24] The other neutral acceptor center, C3, was reported for GaAs:Mn,[21] InP:Mn.[26]

For GaMnN the situation is particularly interesting since Mn acceptor level $A^{-/0}$ ($Mn^{2+/3+}$) is located deep in the band gap of GaN.[27–29] As a result, the nature of Mn impurity will strongly depend on mutual position of the $Mn^{2+/3+}$ and Fermi levels (Fig. 1). For *n*-type samples the Fermi level may be above the $A^{-/0}$ ($Mn^{2+/3+}$) level, which is therefore occupied (Fig. 1) and forces Mn ions into a d^5 configuration. On the other hand for *p*-type samples the Fermi level is below $A^{-/0}$,

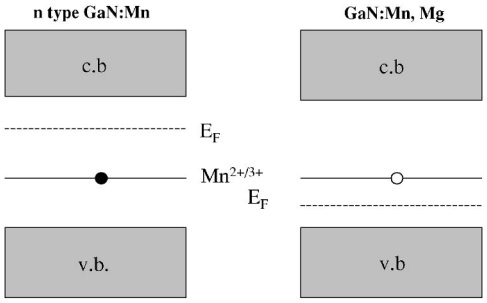

FIG. 1. A scheme presenting the influence of the Fermi level position on the charge state of Mn ion in GaN:Mn crystals.

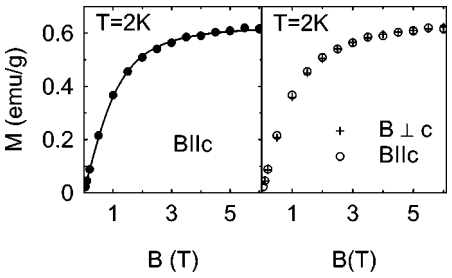

FIG. 2. Magnetization of GaN:Mn as a function of the magnetic field at $T=2$ K. The points in the left-hand panel represent experimental data for B$\|$**c**. The solid line shows the calculated Brillouin function for $S=5/2$ and $x=0.2\%$. On the right-hand panel a comparison of magnetization measured for parallel and perpendicular orientation of the magnetic field referred to the *c* axis is shown.

which is empty and Mn ions should be in d^4 configuration (Fig. 1). Recent optical studies of *n*-type GaN:Mn and highly resistive GaN:Mn, codoped with Mg (a well-known acceptor in the case of GaN) strongly suggest that tuning Fermi level in GaMnN indeed results in switching from d^5 into d^4 configuration.[27]

In this paper we focus on the magnetic aspect of the aforementioned problem. We present magnetization measurements of GaN:Mn, codoped with Mg, as well as *n*-type GaN:Mn (see our preliminary data in Ref. 30). Both systems were chosen with low concentration of Mn ions in order to produce clear results concerning the nature of Mn centers. *n*-GaN:Mn shows isotropic paramagnetic behavior, typical for a spin-only magnetic moment expected for d^5 configuration. In contrast, GaN:Mn,Mg reveals strong magnetic anisotropy. It will be shown that the experimental data can be successfully interpreted assuming Mn in the d^4 configuration. This interpretation is consistent with the conclusions of Refs. 27 and 30.

II. EXPERIMENT

Bulk, single crystals of GaMnN and GaMnN:Mg were grown at the High Pressure Research Center (Warsaw) by an equilibrium high pressure technique from nitrogen solution in liquid gallium. Manganese and magnesium were added into gallium during the growth. The growth was performed under high pressure of N_2 ($p\approx 1.5$ GPa) and at elevated temperature $T\approx 1500\,^\circ$C.[31] Platelets with a diameter of about a few millimeters and thickness of about 100 μm, with wurtzite (2H) structure and *c* axis perpendicular to the crystal plane, were grown. As for GaMnN:Mg we used the same samples which are reported in Ref. 27.

The concentration of Mn in the studied samples was evaluated by secondary ion mass spectroscopy (SIMS) and ranged from 0.0005 to 0.2 mol % depending on the growth conditions. This result is consistent with concentration deduced, in an indirect way, from magnetization data, described below. The low Mn concentration means that more than about 99% of Mn ions have no nearest magnetic neighbors. Thus it is reasonable to consider Mn ions as single, noninteracting magnetic centers.

The *n*-type GaN:Mn samples reveled metallic conductivity with a concentration of free electrons $n\approx 10^{19}$ cm^{-3}. Electron paramagnetic resonance (EPR) experiment showed a resonance, originating from manganese occupying a gallium site in Mn^{2+} (d^5) configuration, in all the *n*-type GaN:Mn. On the other hand GaN:Mn,Mg single crystals were highly resistive with $\rho\sim 10^9\ \Omega$ cm at room temperature. EPR resulting from substitutional Mn^{2+} (d^5) configuration was still observed but its amplitude was about 5–10 times weaker than in GaN:Mn, while the two compared crystals had similar Mn content, i.e., $x=0.01\%$ and 0.009% for GaN:Mn and GaN:Mn,Mg, respectively. In terms of the manganese acceptor level, it means that the Fermi level in GaN:Mn,Mg is placed close to $A^{-/0}$. Moreover, a characteristic absorption band appears at the absorption spectra of highly resistive GaN:Mn,Mg samples, in contrast with GaN:Mn. This band was assigned to the internal transition within the neutral configuration of Mn (for more details see Ref. 27).

The samples' magnetization was measured as a function of magnetic field (up to 6 T) and temperature (2–300 K) using a superconducting quantum interference device (SQUID) magnetometer. In order to have samples of appropriate masses ($\sim$50 mg) a few platelets (5–8) were sandwiched with the use of diamagnetic glue. The magnetic field was applied in perpendicular or parallel orientation to the GaN hexagonal *c* axis. Magnetization data were corrected for the diamagnetism of the GaN host lattice and the glue.

III. RESULTS

Representative magnetization data for *n*-type samples are depicted in Fig. 2, where magnetization as a function of magnetic field is shown. Typical Brillouin-type paramagnetism is observed, with magnetization isotropic within experimental accuracy (Fig. 2). The data can be well-described by the standard Brillouin function with spin $S=5/2$ and Mn ion content $x=0.2\%$ (solid line on the left-hand panel in Fig. 2). Such behavior is exactly as expected for d^5 configuration, for which the ground state of Mn^{2+} ion is an orbital singlet and spin sextet. Such a state is spherically symmetric and thus is insensitive to surrounding ligands, which leads to observed magnetic isotropy.

Magnetic behavior of samples codoped with Mg is essentially different. The data cannot be described by Brillouin

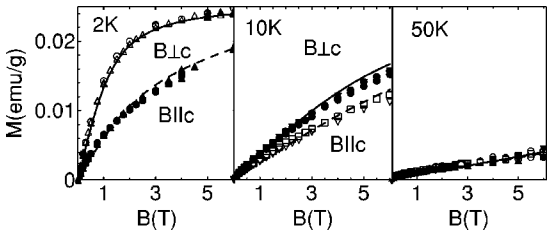

FIG. 3. Magnetization of GaN:Mn codoped with Mg as a function of the magnetic field, for two orientations of the magnetic field referred to *c* axis, at $T=2$, 10, and 50 K. The solid and dashed lines show the magnetization curves calculated due to crystal field model (Table I, parameter set No. 2).

function with $S=5/2$. At the lowest temperatures pronounced anisotropy (ranging to about 50% at $B=2$ T and $T=2$ K) is observed, with the crystal *c*-hexagonal axis being a hard axis (Fig. 3). The anisotropy decreases with increasing temperature and becomes negligible above 50 K (Fig. 3). The observed anisotropy suggests a nonspherical ground state of Mn ion, i.e., a configuration different from d^5 (although in hexagonal surrounding anisotropy for d^5 configuration can in principle be expected, but it is negligible in our temperature range, Ref. 32). Although different electronic configurations $(d^4, d^3, \ldots)$ can yield anisotropic magnetization, we follow the suggestions of Ref. 27, that the dominant Mn configuration in GaN:Mn,Mg is Mn^{3+} (d^4) and interpret the data accordingly. Since concentration of Mn^{2+} ions was not known with reasonable accuracy, in a first attempt to retrieve experimental data we refrained from subtracting their contribution from measured magnetization. This problem will be discussed in the last section.

For the sake of completeness we recall below the model successfully used to describe magnetic properties of d^4 configuration.[20]

IV. THE MODEL

Calculations of magnetization require knowledge about the Mn center energy structure. For d^4 configuration energy structure can be described by the crystal field model developed for Cr^{2+} by Vallin *et al.*[18,19] and then successfully used for Cr-doped cubic and hexagonal II-VI semiconductors.[20,33] We recall that this model takes into account tetrahedral cubic field, spin-orbit interaction, static tetragonal Jahn-Teller distortion, and magnetic field. In the case of hexagonal crystals (e.g., GaN) hexagonal crystal field is also included. It is simulated by a trigonal distortion, along the $\langle 111\rangle$ cubic direction, which is considered as the *c* axis. The energy structure of a single ion in d^4 configuration is then described by the Hamiltonian:

$$H = H_{\mathrm{CF}} + H_{\mathrm{JT}} + H_{\mathrm{TR}} + H_{\mathrm{SO}} + H_{\mathrm{B}}, \tag{1}$$

where H_{CF} is the cubic crystal field tetrahedral symmetry (T_d), H_{TR} is the trigonal crystal field along the *c* axis, which lowers the symmetry to C_{3V}, H_{JT} represents the static Jahn-Teller distortion of tetragonal symmetry, H_{SO} is the spin-orbit coupling, and H_{B} is the Zeeman term representing the effect

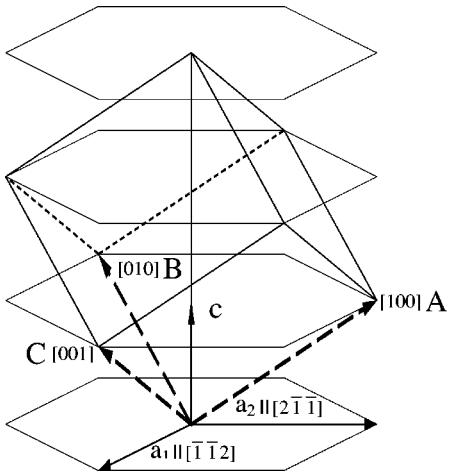

FIG. 4. Schematic picture showing the three distortion axes referred to the *c*-axis of hexagonal lattice.

of magnetic field. The three first terms of the Hamiltonian can be expressed with a use of Stevens equivalent operators:[34]

$$H_{\mathrm{CF}} = -\frac{2}{3}B_4(\hat{O}_4^0 - 20\sqrt{2}\hat{O}_4^3),$$

$$H_{\mathrm{JT}} = \tilde{B}_2^0\hat{\Theta}_4^0 + \tilde{B}_4^0\hat{\Theta}_4^2, \tag{2}$$

$$H_{\mathrm{TR}} = B_2^0\hat{O}_4^0 + B_4^0\hat{O}_4^2,$$

where $\hat{\Theta}$ and $\hat{O}$ are the Stevens operators for tetragonal distortion along the $\langle 100\rangle$ axis and trigonal axis $\langle 111\rangle \| c$ (in hexagonal lattice) and $B_m^n, \tilde{B}_m^n$ are parameters. Here $\hat{\Theta}$ are operators of tetragonal distortion along the $\langle 100\rangle$ axis (Fig. 4) rewritten in the basis for which $\langle 111\rangle$ is the quantization axis (coinciding with the *c* axis).

The first term of Hamiltonian (1) splits the free ion ground state into a tenfold orbital doublet ^5E and 15-fold orbital triplet ^5T, which is the ground term (Fig. 5). The $^5E - {}^5T$ splitting is the crystal field splitting $\Delta = 120\, B_4$. A static tetragonal Jahn-Teller distortion lowers the local symmetry and lifts the degeneracy of the ground term ^5T. This distortion is equivalent to a stress along one of the $\langle 100\rangle$ crystal axes and results in ^5T term splitting into fivefold degenerate orbital singlet ^5B and (located higher) orbital doublet ^5E (Fig. 5). We note that Jahn-Teller distortion creates three kinds of Mn centers in the crystal: center A distorted along [100], center B distorted along [010], and center C distorted along [001] (Fig. 4). In the absence of magnetic field these centers are equivalent and they all are equally probable. Trigonal field splits the ^5E orbital doublet into the two orbital singlets and slightly decreases energy of the ^5B orbital singlet. Trigonal field does not favor any of the centers A, B, and C.

The spin-orbital term in Hamiltonian is $H_{\mathrm{SO}} = \lambda \cdot \mathbf{L} \cdot \mathbf{S}$, where $\mathbf{L}$ and $\mathbf{S}$ are the orbital and spin momentum operators, and λ is the spin-orbit parameter. In general, to take into account the fact that the hybridization of the *d* wave function

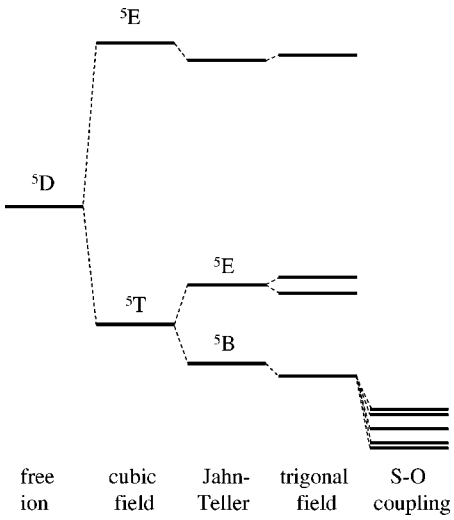

FIG. 5. Scheme of the splittings of the ^5D state of a Mn^{3+} ion in the absence of the magnetic field. The energy level scheme results from tetrahedral cubic field, tetragonal Jahn-Teller distortion, trigonal crystal field, and spin-orbit coupling. The energy level scheme is not in scale.

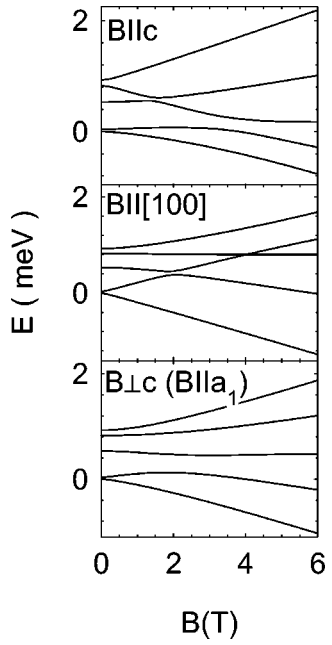

FIG. 6. The calculated energy of the five lowest levels for *A*-type center as a function of magnetic field parallel (top panel) and perpendicular (bottom panel) to the hexagonal *c* axis and collinear with the distortion axes (middle panel).

with the ligands' wave functions is different for the ^5T and ^5E terms the three different parameters, λ_{TT}, λ_{TE}, and λ_{EE}, instead of the single λ parameter are used in computation. The three parameters are defined as follows:

$$\langle \Psi_T|H_{\mathrm{SO}}|\Psi_T\rangle = \lambda_{TT}\langle \Psi_T|\mathbf{L}\cdot\mathbf{S}|\Psi_T\rangle,$$

$$\langle \Psi_T|H_{\mathrm{SO}}|\Psi_E\rangle = \lambda_{TE}\langle \Psi_T|\mathbf{L}\cdot\mathbf{S}|\Psi_E\rangle, \qquad (3)$$

$$\langle \Psi_E|H_{\mathrm{SO}}|\Psi_E\rangle = \lambda_{EE}\langle \Psi_E|\mathbf{L}\cdot\mathbf{S}|\Psi_E\rangle,$$

where Ψ_E and Ψ_T are the wave functions of the ^5E and ^5T subspaces, respectively. The spin-orbit interaction splits the ^5B state into five singlets (the lowest two states are close enough to be regarded as semidoublet in our temperature range).

The effect of an external magnetic field is described by the Zeeman term $H_{\mathrm{B}}=\mu_{\mathrm{B}}(\mathbf{L}+2\cdot\mathbf{S})\cdot\mathbf{B}$, where μ_{B} is the Bohr magneton and **B** is the magnetic field vector. The Zeeman term lifts all the remaining degeneracies. Magnetic field applied along a particular direction distinguishes centers A, B, and C, as in general mutual orientation of Jahn-Teller distortion and magnetic field is different for different centers. Only for **B** directed along [111] centers A, B, and C are equivalent. On the other hand for **B** along $[2\bar{1}\bar{1}]$ ($\mathbf{a}_2$ direction) centers B and C are equivalent but different from center A (Fig. 4).

As the basis for the 25-fold degenerate ^5D term products of the orbital states $\varphi_n=|L,\ L_z\rangle$ and spin states $\chi_m=|S,\ S_z\rangle$ were chosen. The eigenenergies, as well as eigenstates then were calculated by numerical diagonalization of the full 25×25 Hamiltonian (1) matrix. Thus all the interactions were fully taken into account, without any approximations. The Hamiltonian matrix is parameterized by seven parameters: $B_4, B_2^0, B_4^0, \tilde{B}_2^0, \tilde{B}_4^0$, λ_{TT}, and λ_{TE} (final results do not depend on λ_{EE} since the spin-orbit matrix elements relevant to λ_{EE} vanish). Figure 6 displays an example energy level diagram of the lowest five levels for center A, and for the parameters tabulated in Table I, set No. 2. The magnetic field was applied along the hexagonal *c* axis (top panel), along JT distortion (middle panel), and perpendicularly to hexagonal *c* axis

TABLE I. Parameters $B_4, B_2^0, B_4^0, \tilde{B}_2^0, \tilde{B}_4^0$, λ_{TT}, λ_{TE}, $x_{\mathrm{Mn}^{3+}}$, and $x_{\mathrm{Mn}^{2+}}$ used in the magnetization calculations for GaN:Mn,Mg. The second row contains the set of parameters describing the anisotropy of CdS:Cr (taken from Ref. 20). All parameters' values are in meV.

Parameter set No.	B_4	B_2^0	B_4^0	$\tilde{B}_2^0$	$\tilde{B}_4^0$	λ_{TT}	λ_{TE}	$x_{\mathrm{Mn}^{3+}}$ [%]	$x_{\mathrm{Mn}^{2+}}$ [%]
1[a]	5.0	0.23	−0.16	−5.80	−1.16	1.73	6.0		
2	11.44	4.33	−0.56	−5.80	−1.16	3.5	12.5	0.0099	0
3[b]	11.44	4.00	−0.56	−5.25	−1.05	6.5	10	0.0068	0.0022
4	11.44	4.00	−0.56	−5.25	−1.05	4.0	12.5	0.00870	0.00087

[a]CdS:Cr, Ref. 20.
[b]Reference 36.

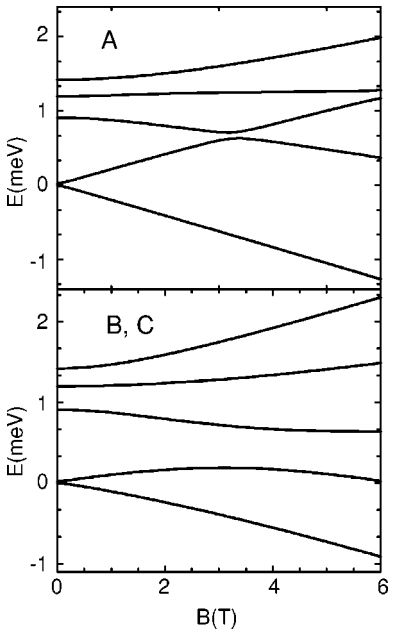

FIG. 7. Calculated energy levels for the A-type (top panel) and B, C-type (bottom panel) centers in magnetic field applied perpendicularly to the c axis ($B \| a_2$).

(bottom panel). The mixing between levels is clearly visible. The difference between centers A, B, and C is exemplified in Fig. 7 for the magnetic field perpendicular to the hexagonal c axis.

Numerical solution of Hamiltonian (1) allows one to calculate the magnetic moment and then to evaluate magnetization for a given concentration of Mn ions. Magnetization per unit mass along the chosen direction γ is the product of the mean magnetic moment of an ion and the number of the ions in the crystal:

$$\mathbf{M}_\gamma = -\frac{\mu_B N_{Av}}{m_{mole}} x \langle \mathbf{L} + 2 \cdot \mathbf{S} \rangle_\gamma, \tag{4}$$

where $\langle \mathbf{L}+2\cdot\mathbf{S}\rangle_\gamma$ is the average magnetic moment of the Mn^{3+} ion along the γ direction, m_{mole} is the molar mass of the GaMnN "molecule," N_{Av} is Avogadro number, and x is the fraction of magnetic ions substituting gallium ions. Since there are in general three different Mn centers in the crystal the average magnetic moment will be composed of magnetic moments of centers A, B, and C. The contribution of each center is proportional to the probability of finding such a center for a given magnetic field. Following the suggestions of Ref. 35 full thermal equilibrium of the system was assumed and $\langle \mathbf{M} \rangle_\gamma$ was calculated with the following formula:[33]

$$\langle \mathbf{M} \rangle_\gamma = Z^{-1}(Z_A \langle \mathbf{M} \rangle_\gamma^A + Z_B \langle \mathbf{M} \rangle_\gamma^B + Z_C \langle \mathbf{M} \rangle_\gamma^C), \tag{5}$$

where Z_n is the partition functions of n center, n=A, B, or C, for a given magnetic field and temperature [$Z_n = \Sigma_i \exp(-E_i^n / k_B T)$], $Z = Z_A + Z_B + Z_C$. The average magnetic moment $\langle \mathbf{M} \rangle_\gamma^n$ of Mn^{3+} ion (in μ_B units) is the thermodynamical average of the magnetic moment operator:

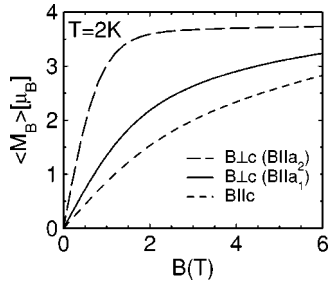

FIG. 8. Calculated magnetic moment of a single Mn^{3+} (d^4) ion for A-type center as a function of magnetic field for three chosen directions of the magnetic field.

$$\langle M \rangle_\gamma^n = \frac{-\sum_{i=1}^N \langle \varphi_i | \hat{L} + 2\hat{S} | \varphi_i \rangle_\gamma \exp(-E_i^n / k_B T)}{\sum_{i=1}^N \exp(-E_i^n / k_B T)}, \tag{6}$$

where E_i^n and φ_i are an ith energy level and corresponding eigenstate of Mn^{3+} ion n-type center. The example magnetic moment of center A is depicted in Fig. 8 for a magnetic field parallel and perpendicular to the crystal hexagonal axis. A large difference in magnetic moment for different orientations of the magnetic field in the plane perpendicular to the hexagonal c axis is visible. It should be noted that this in-plane anisotropy occurs only for a single center. Calculation of total mean magnetic moment given by Eq. (5), i.e., averaging over centers A, B, and C, yields practically isotropic in-plane magnetization. However, the difference between parallel (relative to the c axis) and perpendicular magnetization is still large. We conclude that the magnetic anisotropy of the $Mn^{3+}(d^4)$ system originates from the hexagonal axial field along the c axis and different distributions of nonequivalent Jahn-Teller centers in two orientations of magnetic field.

V. DISCUSSION

Applying the above-presented model to experimental magnetization data one should be aware of two issues. The first one is the large number of parameters in the model. The second one is a non-negligible magnetic contribution resulting from $Mn^{2+}(d^5)$ $S=5/2$ detected in the EPR experiment, mentioned above (see Sec. II). The latter contribution is described by a standard Brillouin function (Sec. III) and could be easily taken into account provided the exact concentration of Mn^{2+} ions is known. Unfortunately only the rough estimation of this parameter is available (rather the ratio between Mn^{3+}/Mn^{2+} estimated from EPR). In such a situation it is essential to limit the number of free parameters and to proceed step by step with the fit to control the role played by each parameter.

Therefore as a first approach we decided to fit the raw magnetization data (i.e., including Mn^{2+} contribution, Fig. 3) by pure d^4 model [Eq. (5)], i.e., neglecting Mn^{2+} contribution. Moreover, since little was known about parameters of the model for the particular case of GaN, as starting parameters the values reported for Cr^{2+} (d^4) in CdS (Ref. 20) were used for $B_2^0, B_4^0, \tilde{B}_2^0, \tilde{B}_4^0$, λ_{TT}, and λ_{TE} (Table I, parameter set

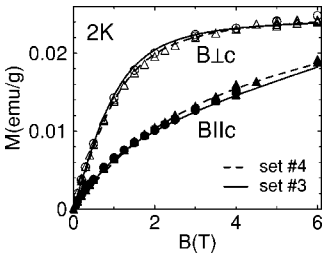

FIG. 9. Magnetization of GaN:Mn,Mg as a function of the magnetic field, for two orientations of the magnetic field at $T=2$ K. The solid and dashed lines represent magnetization calculated with the use of parameter set No. 3 and parameter set No. 4 (Table I), respectively.

No.1). For ^5B we used 11.44 meV, the value obtained from experimentally observed crystal field splitting in GaN:Mn.[27] The value of B_4 was then kept constant during the fit. Performing the calculations we noticed that the magnitude of the anisotropy is very sensitive to spin-orbit and trigonal field parameters values, while the influence of the Jahn-Teller parameters on the final result is much smaller. It was found that all the data can be reasonably well described (see Fig. 3) by the set of parameters collected in Table I (parameter set No.2). Although the obtained parameter (set No.2) should be regarded as a sample one, due to neglect of Mn^{2+} contribution, the obtained result demonstrate that the d^4 model is able to recover characteristic features of GaN:Mn,Mg magnetization.

In the next step the contribution of Mn^{2+} ions was taken into account. The measured magnetization (Fig. 3) was then assumed to be composed of Mn^{3+} and Mn^{2+} contributions, i.e., mean magnetic moment was described by the formula:

$$\langle M\rangle = x_{\mathrm{Mn}^{3+}}\langle M_{\mathrm{Mn}^{3+}}\rangle + x_{\mathrm{Mn}^{2+}}\langle M_{\mathrm{Mn}^{2+}}\rangle \qquad (7)$$

where $\langle M_{\mathrm{Mn}^{2+}}\rangle$ is given by a Brillouin function with $S=5/2$ and $x_{\mathrm{Mn}^{3+}}$, $x_{\mathrm{Mn}^{2+}}$ are additional adjustable parameters. Only slight modifications (less than 10% in most cases) of previous crystal field parameters, set No.2, were necessary to obtain a reasonable fit with Mn^{3+} and Mn^{2+} centers. If one chooses exactly the same parameters as recently obtained from analysis of magnetospectroscopy experiment,[36] where infrared (IR) transitions between ^5T and ^5E terms were observed and successfully described by the d^4 model (Table I, parameter set No.3), the values $x_{\mathrm{Mn}^{3+}}=0.0068$ and $x_{\mathrm{Mn}^{2+}}=0.0022$ were returned (Table I, set No.3, Fig. 9). The obtained abundance of Mn^{2+} may be too high in respect of EPR data mentioned above. Fixing the ratio $x_{\mathrm{Mn}^{3+}}/x_{\mathrm{Mn}^{2+}}$ on the level of 10/1, as suggested by EPR, one obtains an equally good fit (Fig. 9) for slightly different spin-orbit interaction parameters (Table I, parameter set No.4). The difference in parameters of sets No.3 and No.4 is not large and in our opinion is irrelevant, as the ratio $x_{\mathrm{Mn}^{3+}}/x_{\mathrm{Mn}^{2+}}$ is known with poor accuracy. We stress that the model parameters obtained with the above fits should be treated with caution. Calculating magnetization means in fact averaging over different energy levels and different configurations (A, B, and C centers), so the energy structure is probed in an indirect way. In this regard we would favor parameter set No.3, as this is the optimal one for both magnetic and IR spectroscopy data.

A much more reliable way to determine these parameters is far infrared (FIR) magnetospectroscopy, which probes low energy levels of the ground term (precisely the lowest five levels) and enables direct comparison of calculated energy levels and measured transition energies. The set of energies of several transition energies is usually critically sensitive to the model parameters.[37] Unfortunately the appropriate FIR data are unavailable.

Nevertheless, it seems apparent that the model of Mn in the d^4 configuration *can* satisfactory describe magnetization of our GaN:Mn,Mg samples, which supports results of optical experiments discussed in Refs. 27 and 36. However, the other possibilities (different d^n configurations) are not excluded. To make this conclusion more pertinent further experiments should be performed. In particular the structure of the lowest levels should be precisely established by FIR magnetospectroscopy.

VI. CONCLUSIONS

The magnetic properties of bulk GaN:Mn and GaN:Mn codoped with Mg, grown by the equilibrium high pressure method, were investigated. Magnetization measurements performed on these crystals revealed strong dependence of the Fermi level position, yielding differences of the Mn impurity nature. Magnetization of the *n*-type GaN:Mn is well described by the standard Brillouin function with spin 5/2 resulting from d^5 configuration of Mn^{2+} ions. In contrast, GaN:Mn codoped with Mg, which lowers the Fermi level, reveals strong magnetic anisotropy. Our calculations show that the observed anisotropy can be well understood in terms of nonspherical d^4 configuration of Mn ions. The crystal field model of the d^4 configuration was successfully used to reproduce the magnetization data of GaN:Mn,Mg crystals. The results of this work are consistent with spectroscopy results presented in Refs. 27 and 36. Observation of Mn in the d^4 configuration rises the hopes for an alternative mechanism for ferromagnetic coupling between Mn ions in GaN, not necessarily requiring high concentration of free holes. Experimental verification of this hypothesis requires GaMnN crystals with substantially higher concentration of manganese ions in d^4 configuration (few molar percent), which is probably a challenging task.

ACKNOWLEDGMENTS

This work was partially supported under the project FENIKS (G5RD-CT-2001-2001-00535) and partially by the State Committee for Scientific Research (Poland), in particular under Grant No. PBZ-KBN-044/P03/2001.

*Electronic address: gosk@fuw.edu.pl

[1] S. A. Wolf, D. D. Awschalom, R. A. Buhrman, J. M. Daughton, S. von Molnar, M. L. Roukes, A. Y. Chtchelkanova, and D. M. Treger, Science **294**, 1488 (2001).
[2] H. Ohno, H. Munekata, T. Penney, S. von Molnar, and L. L. Chang, Phys. Rev. Lett. **68**, 2664 (1992).
[3] F. Matsukura, H. Ohno, A. Shen, and Y. Sugawara, Phys. Rev. B **57**, R2037 (1998).
[4] T. Dietl, H. Ohno, F. Matsukura, J. Cibert, and D. Ferrand, Science **287**, 1019 (2000).
[5] T. Sasaki, S. Sonoda, Y. Yamamoto, K. Suga, S. Shimizu, K. Kindo, and H. Hori, J. Appl. Phys. **91**, 7911 (2002).
[6] N. Theodoropoulou, A. F. Hebard, M. E. Overberg, C. R. Abernathy, S. J. Pearton, S. N. G. Chu, and R. G. Wilson, Appl. Phys. Lett. **78**, 3475 (2001).
[7] M. L. Reed, N. A. El-Masry, H. H. Stadelmaier, M. K. Ritums, M. J. Reed, C. A. Parker, J. C. Roberts, and S. Bedair, Appl. Phys. Lett. **79**, 3473 (2001).
[8] M. N. Overberg, R. Cammy, R. Abernathy, S. J. Pearton, N. Theodoropoulou, K. T. MacCarthy, and A. F. Hebard, Appl. Phys. Lett. **79**, 1312 (2001).
[9] M. Zajac, J. Gosk, E. Grzanka, M. Kaminska, A. Twardowski, B. Strojek, T. Szyszko, and S. Podsiadlo, J. Appl. Phys. **93**, 4715 (2003).
[10] S. Kuwabara, K. Ishii, S. Haneda, T. Kondo, and H. Munekata, Physica E (Amsterdam) **10**, 233 (2001).
[11] S. Dhar, O. Brandt, A. Trampert, K. J. Friedland, Y. J. Sun, and K. H. Ploog, Phys. Rev. B **67**, 165205 (2003).
[12] K. Sato and H. Katayma-Yoshida, Jpn. J. Appl. Phys., Part 2 **40**, L485 (2001).
[13] H. Katayama-Yoshida, R. Kato, and T. Yamamoto, J. Cryst. Growth **231**, 428 (2001).
[14] M. van Schilfgaarde and O. N. Mryasov, Phys. Rev. B **63**, 233205 (2001).
[15] E. Kulatov, H. Nakayama, H. Mariette, H. Ohta, and Yu. A. Uspenskii, Phys. Rev. B **63**, 045203 (2002).
[16] L. Kronik, M. Jain, and J. R. Chelikowsky, Phys. Rev. B **66**, 041203(R) (2002).
[17] T. Dietl, F. Matsukura, and H. Ohno, Phys. Rev. B **66**, 033203 (2002).
[18] J. T. Vallin, G. A. Slack, S. Roberts, and A. E. Hughes, Phys. Rev. B **2**, 4313 (1970).
[19] J. T. Vallin and G. D. Watkins, Phys. Rev. B **9**, 2051 (1974).
[20] M. Herbich, W. Mac, A. Twardowski, K. Ando, Y. Shapira, and M. Demianiuk, Phys. Rev. B **58**, 1912 (1998).
[21] J. Schneider, U. Kaufmann, W. Wilkening, M. Baeumler, and F. Köhl, Phys. Rev. Lett. **59**, 240 (1987).
[22] J. Szczytko, A. Twardowski, K. Swiatek, M. Palczewska, M. Tanaka, T. Hayashi, and K. Ando, Phys. Rev. B **60**, 8304 (1999).
[23] J. Szczytko, A. Twardowski, M. Palczewska, R. Jablonski, J. Furdyna, and H. Munekata, Phys. Rev. B **63**, 085315 (2001).
[24] J. Kreissl, W. Ulrici, M. El-Metoui, A. M. Vasson, A. Vasson, and A. Gavaix, Phys. Rev. B **54**, 10 508 (1996).
[25] M. Zajac, R. Doradzinski, J. Gosk, J. Szczytko, M. Lefeld-Sosnowska, M. Kaminska, A. Twardowski, M. Palczewska, E. Grzanka, and W. Gebicki, Appl. Phys. Lett. **78**, 1276 (2001).
[26] B. Lambert, B. Clerjaud, C. Naud, B. Deveaud, G. Picoli, and Y. Toudic, in *Proceedings of the Thirteenth International Conference on Defects in Semiconductors, 1985*, edited by L. K. Kimerling and J. M. Parsey (Metallic Society, AIME, Warrendale, PA), p. 1141.
[27] A. Wołoś, M. Palczewska, M. Zajac, J. Gosk, M. Kaminska, A. Twardowski, M. Bockowski, I. Grzegory, and S. Porowski, Phys. Rev. B **69**, 115210 (2004).
[28] T. Graf, M. Gjukic, M. S. Brandt, M. Stutzmann, and O. Ambacher, Appl. Phys. Lett. **81**, 5159 (2002).
[29] R. Y. Korotkov, J. M. Gregie, B. Han, and B. W. Wessels, Physica B **308**, 30 (2001).
[30] J. Gosk, M. Zajac, M. Kaminska, A. Twardowski, I. Grzegory, M. Bockowski, and S. Porowski, Acta Phys. Pol. A **103**, 665 (2003).
[31] I. Grzegory, J. Phys.: Condens. Matter **13**, 6875 (2001).
[32] C. D. Amarasekara, R. R. Gałązka, Y. Q. Yang, and P. H. Keesom, Phys. Rev. B **27**, 2868 (1983).
[33] W. Mac, A. Twardowski, P. J. T. Eggenkamp, H. J. M. Swagten, Y. Shapira, and M. Demianiuk, Phys. Rev. B **50**, 14 144 (1994).
[34] A. Abragam and B. Bleaney, *Electron Paramagnetic Resonance of Transition Metal Ions* (Clarendon Press, Oxford, 1970).
[35] G. H. McCabe, Y. Shapira, V. Bindilatti, N. F. Oliveira, A. Twardowski, W. Mac, E. J. McNiff, and M. Demianiuk, Solid State Commun. **95**, 841 (1995).
[36] A. Wolos, A. Wysmolek, M. Kaminska, A. Twardowski, M. Bockowski, I. Grzegory, S. Porowski, and M. Potemski, Phys. Rev. B **70**, 245202 (2004).
[37] R. Krevet, A. Twardowski, M. von Ortenberg, W. Mac, and M. Demianiuk, Solid State Commun. **87**, 709 (1993); W. Mac, A. Twardowski, M. E. J. Boonman, A. Wittlin, R. Krevet, M. von Ortenberg, and M. Demianiuk, Physica B **211**, 384 (1995); M. E. J. Boonman, W. Mac, A. Twardowski, A. Wittlin, P. J. M. van Bentum, J. C. Maan, and M. Demianiuk, Phys. Rev. B **61**, 5358 (2000).